Nano Research
2022, 15(5): 4327–4333

ISSN 1998-0124 CN 11-5974/O4
https://doi.org/10.1007/s12274-021-4034-3

Research Article

Modulation of electronic state in copper-intercalated 1T-TaS_2

Wenhao Zhang[1,§], Degong Ding[2,§], Jingjing Gao[3,§], Kunliang Bu[1], Zongxiu Wu[1], Li Wang[4], Fangsen Li[4], Wei Wang[3], Xuan Luo[3], Wenjian Lu[3], Chuanhong Jin[2] (✉), Yuping Sun[3,5,6] (✉), and Yi Yin[1,6] (✉)

[1] *Zhejiang Province Key Laboratory of Quantum Technology and Device, Department of Physics, Zhejiang University, Hangzhou 310027, China*
[2] *State Key Laboratory of Silicon Materials, School of Materials Science and Engineering, Zhejiang University, Hangzhou 310027, China*
[3] *Key Laboratory of Materials Physics, Institute of Solid State Physics, HFIPS, Chinese Academy of Sciences, Hefei 230031, China*
[4] *Vacuum Interconnected Nanotech Workstation (Nano-X), Suzhou Institute of Nano-Tech and Nano-Bionics (SINANO), Chinese Academy of Sciences (CAS), Suzhou 215123, China*
[5] *High Magnetic Field Laboratory, HFIPS, Chinese Academy of Sciences, Hefei 230031, China*
[6] *Collaborative Innovation Center of Advanced Microstructures, Nanjing University, Nanjing 210093, China*
[§] *Wenhao Zhang, Degong Ding, and Jingjing Gao contributed equally to this work.*

Received: 9 October 2021 / **Revised:** 15 November 2021 / **Accepted:** 30 November 2021

ABSTRACT

Intercalation is an effective method to modify physical properties and induce novel electronic states of transition metal dichalcogenide (TMD) materials. However, it is difficult to reveal the microscopic electronic state evolution in the intercalated TMDs. Here we successfully synthesize the copper-intercalated 1T-TaS_2 and characterize the structural and electronic modification combining resistivity measurements, atomic-resolution scanning transmission electron microscopy (ADF-STEM), and scanning tunneling microscopy (STM). The intercalated Cu atom is determined to be directly below the Ta atom and suppresses the commensurate charge density wave (CCDW) phase. Two specific electronic modulations are discovered in the near-commensurate (NC) CDW phase: the electron doping state near the defective star of Davids (SDs) in metallic domains and the spatial evolution of the Mott gap in insulating domains. Both modulations reveal that intercalated Cu atoms act as a medium to enhance the interaction between intralayer SDs, in addition to the general charge transfer effect. It also solidifies the Mott foundation of the insulating gap in pristine samples. The intriguing electronic evolution in Cu-intercalated 1T-TaS_2 will motivate further exploration of novel electronic states in the intercalated TMD materials.

KEYWORDS

intercalation, scanning tunneling microscopy, Mott insulator, charge transfer, electron doping

1 Introduction

The layered transition metal dichalcogenide (TMD) 1T-TaS_2 has been extensively explored due to its extraordinary physical properties [1–8]. At low temperature, it is conventionally considered as a Mott insulator in the commensurate charge density wave (CCDW) state [1–3]. The interplay between electron correlation and electron-phonon interaction, accompanied with the triangular lattice geometry, leads to a rich phase diagram [2–8]. Many exotic electronic states like the superconductor, Anderson insulator, and quantum spin liquid state have been proposed and experimentally explored [4–9]. Recently, the origin of the insulating gap and the strong correlation nature of 1T-TaS_2 have been questioned after considering the stacking-order effect [10–15]. There are revived interests in exploring the electronic state of this material.

Intercalation with metallic atoms is an effective method to tune the physical properties of TMD materials [9, 16–18]. The main effect of intercalation is to increase the interlayer distance and to induce charge transfer with extra electrons [19–24]. In Cu-intercalated 2H-NbS_2, the *c* lattice constant increases from 1.189 to 1.307 nm for $Cu_{0.3}NbS_2$ and further to 1.321 nm for $Cu_{1.2}NbS_2$ [18]. In Cu-intercalated 1T-$TiSe_2$, the charge transfer suppresses the long-range coherent CCDW order and results in a superconductor [21–24]. Intercalating metallic atoms into 1T-TaS_2 is likely to decouple the interlayer interaction and modify the electronic states. We expect the intercalated system to provide more evidence about the interplay of different interactions in the pristine 1T-TaS_2.

We reported a detailed study of the electron doping effect in Cu-intercalated 1T-TaS_2. The Cu atoms were directly visualized between TaS_2 layers and determined to be directly below the Ta atoms in the atomic-resolution scanning transmission electron microscopy (ADF-STEM) measurements. The intercalation slightly increased the interlayer spacing of 1T-TaS_2. The resistivity and scanning tunneling microscopy (STM) measurements revealed that the global charge transfer of Cu atoms destabilizes the long-range coherent CDW order and suppresses the CCDW phase. In the near-commensurate (NC) CDW phase, there were many nano-sized metallic domains. Occasionally, we observed domains with insulating spectra.

In particular, we observed two unique electronic modulations: the enhanced density of states (DOS) around a defective star of David (SD) in metallic domains and the spatial evolution of the

Address correspondence to Chuanhong Jin, chhjin@zju.edu.cn; Yuping Sun, ypsun@issp.ac.cn; Yi Yin, yiyin@zju.edu.cn

Mott gap near a domain wall in insulating domains. The electronic state of the defective SD exhibits suppression of DOS above the Fermi level, identical to the defective SD's spectrum in pristine 1T-TaS_2. Unlike the pristine sample, the DOS on the six nearest SDs shows a substantial enhancement near the Fermi level. We attribute the redistribution of electronic state to increased interaction between SDs in Cu-intercalated systems. We also observe an emergent in-gap state above the Fermi level in an insulating domain near the domain wall. After slowly moving away from the domain wall, the in-gap state gradually fades away, and the upper peak is reestablished. This spatial evolution of DOS is compatible with the electron doping Hubbard scenario.

The exotic electronic modulations demonstrate that a global charge transfer happens from the intercalated Cu atoms to the neighboring TaS_2 layers, suppressing the long-range coherent CDW order. The electron doping induces a Mott-insulator-to-metal transition. Besides the charge transfer, the Cu intercalation also enhances the interaction between intralayer SDs and induces unique modulation of the electronic state.

2 Results and discussion

The TMD 1T-TaS_2 is a long-known CDW material [1, 2]. As shown in Fig. 1(a), the unit structure of 1T-TaS_2 contains a triangular Ta layer sandwiched between two triangular sulfur layers. The material undergoes two CDW phase transitions as the temperature decreases, from incommensurate (IC) to NCCDW state at 350 K and NCCDW state to CCDW state at 180 K (Fig. 1(b)). In the NCCDW and CCDW phase, every 13 Ta atoms shrink into a cluster named as SD. The SD reconstructs to a long coherent $\sqrt{13} \times \sqrt{13}$ triangular super-lattice in the CCDW state (Fig. 1(b)). Each SD contributes one orphan electron, leading to a half-filled flat band near the Fermi level and a relatively strong electron correlation. In the Mott insulator scenario, the half-filled band splits into the upper and lower Hubbard bands, forming a Mott insulating gap around the Fermi level. Different tuning methods have been applied to explore this system's novel and exotic electronic state [5–9].

The Cu-intercalated 1T-TaS_2 was successfully synthesized via the chemical vapor transport (CVT) method (detailed description in sample growth method). The TaS_2 layers were stacked up via the van der Waals interaction. Intercalated Cu atoms reside between TaS_2 layers, as illustrated in Fig. 1(c). The NC/CCDW transition of 1T-TaS_2 is completely suppressed after the Cu intercalation (Fig. 1(d)). The energy dispersive spectroscopy (EDS) determines a rough Cu content of $x = 0.05$ in 1T-Cu_xTaS_2. We did not observe many residue Cu atoms in STM topography (Fig. 1(e)) or the STEM image in (001) direction. Due to a weak van der Waals bonding, intercalated Cu atoms on the surface might scatter into the vacuum in the cleaving process. To determine the location of Cu atoms, we performed the atomic-resolution ADF-STEM measurements. Due to the *Z*-contrast atomic intensity in the STEM image, the Cu atomic columns are dimmer than Ta atomic columns. The atomic-resolved ADF-STEM image (Fig. 1(f)) viewed along the (100) direction shows Cu atomic columns are intercalated into the TaS_2 interlayers. The illustration image is partial zoom-in detail in Fig. 1(g). Detailed cross-section intensity line profile in Fig. 1(h) upper panel suggests the interlayer Ta-Ta distance is slightly expanded from 0.58 to 0.61 nm, demonstrating that the slight lattice expansion is attributed to the intercalation of Cu atoms [18–20]. The distance of the Cu-Cu atomic column and Cu-Ta atomic column is about 0.61 and 0.30 nm, respectively, indicating that the Cu atoms are intercalated into the middle position of TaS_2 interlayers without any obvious offset. In other words, Cu atomic columns are right below the Ta atomic columns, which are also the energetically favorable sites indicated by our density functional theory (DFT) calculations. The Cu column line profile displays the intensity variation of Cu sites, revealing a spatial inhomogeneity of intercalated Cu atoms. Noting that the schematic diagram Fig. 1(c) is drawn corresponding to the visual result of Fig. 1(f), which displays a zone-axis region to see the atomic column. More generally, not all regions are Cu-rich. More STEM images claim a spatial inhomogeneity of Cu atoms at different regions.

We performed detailed scanning tunneling microscopy and spectroscopy (STM/STS) measurements to study the structural and electronic modification in Cu-intercalated 1T-TaS_2. Figure 1(e) displays a 100 nm × 100 nm large area topography. Nano-size domains were observed in the field of view (FOV), consistent with the NCCDW phase in the resistivity result. The domain walls are more distinct under a negative-bias junction. Inside each domain, the bright SDs maintain the triangular super-lattice, despite some dark defective SDs. The suppressed

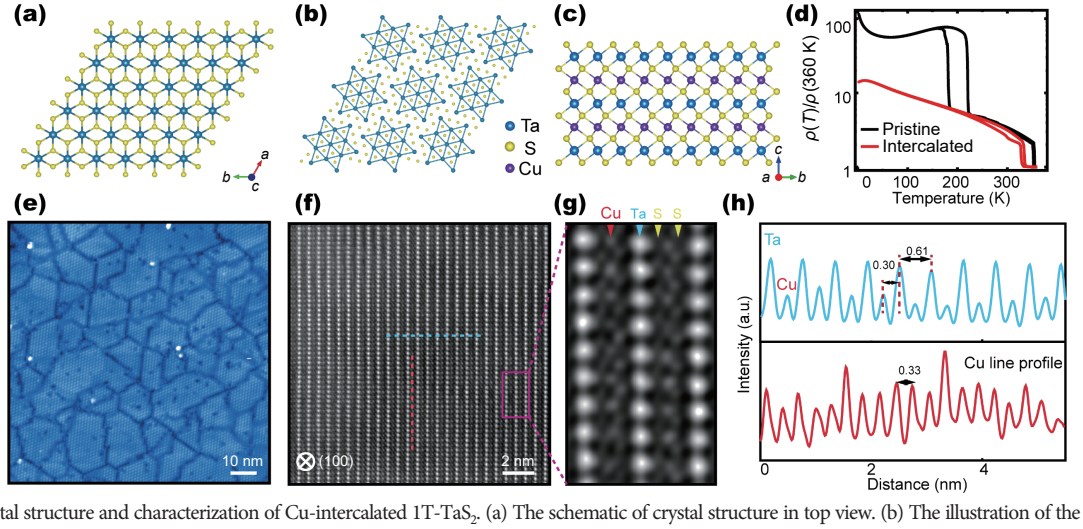

Figure 1 Crystal structure and characterization of Cu-intercalated 1T-TaS_2. (a) The schematic of crystal structure in top view. (b) The illustration of the star of Davids in NC/CCDW phase. Every 13 Ta atoms shrink into a cluster. (c) The side view of Cu-intercalated 1T-TaS_2. Cu atoms are right below the Ta atoms. (d) The temperature dependence of resistivity ratio $\rho(T)/\rho(360\ \mathrm{K})$ for pristine and Cu intercalated samples. (e) A typical 100 nm × 100 nm large topography with small domains in the NCCDW phase ($V_b = -600$ mV, $I_t = 500$ pA, $T = 77$ K). The scattered bright spots may be residual Cu clusters. (f) The atomic resolution ADF-STEM image along (100) direction. (g) The enlarged image after filtering of the purple square area in (f). The sky-blue, yellow, and red arrows indicate the Ta, S, and Cu columns, respectively. (h) The intensity line profile of the interlayer structure and Cu column is indicated by the red and sky-blue dash line in (f), respectively.

long-range CDW order is similar to that in other intercalation TMD materials [22]. Some bright clusters scattered on the surface are possible residual Cu atoms. Most Cu clusters reside near the domain walls or defective SDs, different from the periodic arrangement of Cu atoms between TaS_2 layers. Few left Cu clusters on the surface may be related to the cleave process and the weak bonding between Cu and the underlying TaS_2 layer. Due to the strong electronic modulation of the SDs, it is hard to visualize the inhomogeneous distribution of underlying Cu atoms [22].

Figure 2(a) displays a clean 30 nm × 30 nm area topography with several domains. It exhibits different electronic behavior in different domains (Fig. 2(b)). The most typical dI/dV spectrum shows a V-shaped feature and a nonzero DOS near the Fermi level, suggesting a metallic behavior. Despite the similar V-shaped feature, there are still some slight differences for the dI/dV spectra in different domains, especially the position of the two peaks. The purple curve in Fig. 2(b) shows a two-peak feature for the negative-bias peak. The split of the negative-bias peak has been observed in the stacking-order-induced small-gap spectrum [13, 25]. The insulating domains are occasionally found, like the upper left domain in Fig. 2(a). The corresponding red dI/dV curve exhibits a large insulating gap, similar to that in pristine samples [26]. The negative-bias peak of the insulating spectrum also coincides with the lower peak of the two-peak feature in the metallic spectrum. During our hundreds of measurements, we have identified the insulating domains less than ten times.

Along the solid lines in Fig. 2(a), three series of dI/dV spectra are displayed in Fig. 2(c). In the linecut maps, the periodic oscillation is consistent with the periodicity of SDs. Apart from this periodic variation, the electronic state is relatively homogenous between different supersites inside each domain. The peaks near the Fermi level are most substantial at the center of SDs, whether in metallic or insulating domains. The two peaks of insulating spectra are sharper and relatively farther from the Fermi level than those of metallic spectra. In the middle linecut map, the two-peak feature of the negative-bias peak shares a similar distribution. The linecut maps indicate that the DOS near the Fermi level originates from the central Ta atoms [8]. The different electronic behaviors of domains are related to distinct electron correlation and possible Mott physics. The CDW-related DOS above 300 mV and below −300 mV are most substantial at intermediate regions between SDs. The upper enhancement above 300 mV remains the same in metallic and insulating domains, while the lower enhancement below −300 mV slightly shifts to lower energy in insulating domains. Nevertheless, the CDW-related DOS all originates from the surrounding Ta atoms [8]. The Cu intercalation does not perturb the CDW-related DOS and the electronic homogeneity within domains from the linecut maps. At least from the electronic behavior of metallic domains, we cannot distinguish the Cu-rich and Cu-poor regions.

Intercalation inevitably introduces some disorder into the system. Previous angle-resolved photoemission spectroscopy (ARPES) study suggests a disorder-induced Mott insulator to metal transition in Cu-intercalated 1T-TaS_2 [27]. Our STM results reveal that although the electronic states vary in different domains, the electronic state inside each domain is relatively homogenous. Intercalated Cu atoms introduce universal charge transfer into the TaS_2 layer, which structurally destabilizes the long-range $\sqrt{13} \times \sqrt{13}$ CDW order and induces small domains [22]. We suspect that the electron correlation is relatively unstable in small domains, with the electronic state easily perturbed to be metallic state, etc. [28–30]. Most small domains are metallic, accompanied by metallic domain walls, leading to the macroscopic insulator to metal transition.

The electronic evolution around defective SDs and domain walls provides more evidence of electronic modification in the Cu-intercalated system. The three-petal defective SD has been reported in pristine 1T-TaS_2 [25]. Lacking the central Ta atom in SD suppresses the positive-bias peak and shifts the negative-bias peak to lower energies. The DOS perturbation of the defective SD mainly occurs inside the SD. The DOS of six nearest SDs remains insulating and unperturbed in pristine samples. Similar defective SDs can be observed in Cu intercalated 1T-TaS_2. One such defective SD is marked by a yellow dot in a metallic domain (Fig. 3(a)). Compared with the DOS at normal SDs, the primary

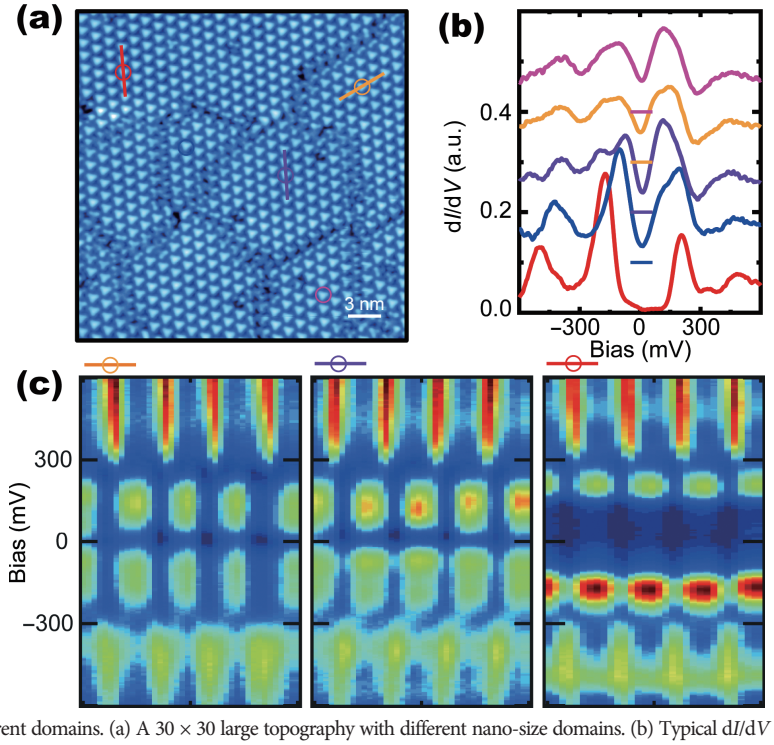

Figure 2 Electronic state in different domains. (a) A 30 × 30 large topography with different nano-size domains. (b) Typical dI/dV spectra of different domains in (a) (V_b = −600 mV, I_t = 500 pA). (c) The linecut maps of dI/dV spectra along the three solid lines in (a).

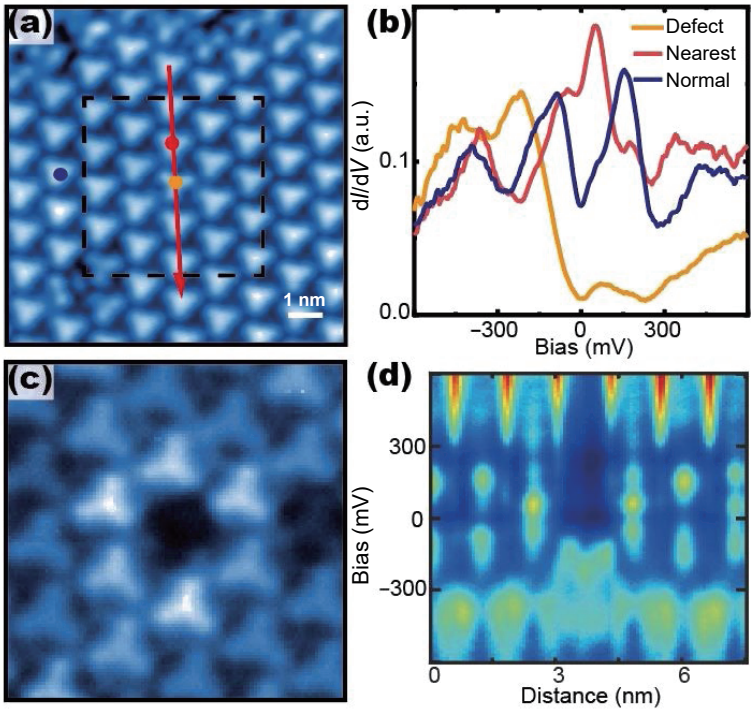

Figure 3 Electronic structure of the defective SD in metallic domains. (a) A 10 nm × 10 nm topography with a defective SD at the center of a metallic domain. (b) Three typical d*I*/d*V* spectra on defective, nearest, and normal SD inside the metallic domain, indicated by yellow, red, and blue dots in (a), respectively (V_b = −600 mV, I_t = 500 pA). (c) The black dash square's d*I*/d*V* conductance map in (a) at the Fermi level. The defective SD exhibits suppressed intensity while the surrounding six SDs display enhanced intensity. (d) The linecut profile of the d*I*/d*V* spectra along the red line in (a).

electronic modification of the defective SD is similar to that in pristine samples, as shown by the yellow curve in Fig. 3(b). It exhibits a strong suppression of the positive-bias peak and a shift of the negative-bias peak. Besides these two major features, the DOS near the Fermi level is strongly suppressed to near-zero value. Unlike the state of nearest SDs in pristine samples, the surrounding six SDs, however, exhibit a substantial enhancement near the Fermi level (red curve in Fig. 3(b)). The DOS enhancement shows an asymmetric two-peak feature within the 100 mV range, and the degree of asymmetry varies for different defective SDs. The split two-peak feature may relate to a complicated charge or spin interaction inside the SDs, with a detailed theoretical explanation beyond our current understanding [31]. A straightforward statement is that there is extra carrier doping at surrounding SDs. The d*I*/d*V* conductance maps and linecut spectra measurements around the defective SD reveal a spatial distribution of the carrier doping state. The d*I*/d*V* map at the Fermi level energy (Fig. 3(c)) displays that the carrier doping state is localized in the nearest six SDs. The linecut d*I*/d*V* spectra also suggest a localized DOS enhancement in the nearest SDs. The second nearest SD exhibits a normal metallic state.

In pristine samples, the orphan electron of the central Ta atom is strongly localized inside the SD. The perturbation of defective SDs is also localized inside the SD, even in metallic domains. Previous X-ray absorption fine structure measurements suggested that the intercalated Cu atoms form bonds with the halogen atoms in TMD materials, resulting in a charge transfer from Cu to halogen (S/Se) atoms [20]. The charge transfer modifies the half-filling system. Our results of defective SD suggested that the intercalated Cu atoms also strengthen the interaction between neighboring SDs. With a local chemical imbalance around the defective SD, the charge transfer between Cu and S atoms redistributes and enhances the DOS of six surrounding SDs.

Another non-local carrier doping effect near the domain wall is found in Cu-intercalated 1T-TaS_2. As discussed in Fig. 2, the insulating state remains in some domains in Cu-intercalated 1T-TaS_2. Figure 4(a) displays a 12 nm × 12 nm insulating domain, with the domain wall residing at the bottom area. The domain wall d*I*/d*V* spectra exhibit an enhanced peak above the Fermi level, similar to the metallic domain wall d*I*/d*V* spectra in pristine samples [32–34]. The d*I*/d*V* conductance map in Fig. 4(b) also exhibits a substantial DOS enhancement at the domain wall, implying the metallic nature of the domain wall. We conduct a linecut d*I*/d*V* spectrum measurement near the metallic domain wall at the dotted SDs. Different from the insulating spectrum, the d*I*/d*V* spectrum of the bottom SD (gray dot) displays a relatively small gap (gray curve in Fig. 4(c)). An in-gap state emerges at 110 mV, while the upper peak at 200 mV is strongly suppressed. As the tip moves away from the domain wall, the lower peak shifts merely lower, without an obvious intensity change. It implies that other valence bands except the central Ta band possibly hybridize with the LHB. The in-gap state at 110 mV keeps decreasing, and the upper peak at 200 mV is gradually enhanced. This phenomenon is very similar to the doped-electron-induced state evolution in the cuprate $Ca_2CuO_2Cl_2$ Mott insulator [35]. It seems that a local doped electron exists within the domain wall area, which triggers the suppressed UHB and emerged in-gap state for SDs close to the domain wall.

To show the two-dimensional distribution of this doped state, Fig. 4(b) displays the d*I*/d*V* map intentionally chosen at 110 mV, the energy of the in-gap state. The conductance of the in-gap state fades away from the domain wall in the d*I*/d*V* map instead of only along the arrowed direction. We extracted the typical d*I*/d*V* spectra at the SD centers and subtract them with the Mott insulating d*I*/d*V* spectrum (yellow curve). As shown in Fig. 4(d), the intensity of the in-gap state and the suppression of the upper peak decrease with increasing distance from the domain wall. Comparing the enclosed area of the two envelopes, we obtained more enhancement of the in-gap state than suppressing the upper peak. It implies some electron doping besides spectra transfer between the in-gap state and the upper peak.

The electron doping evolution is unique in Cu-intercalated

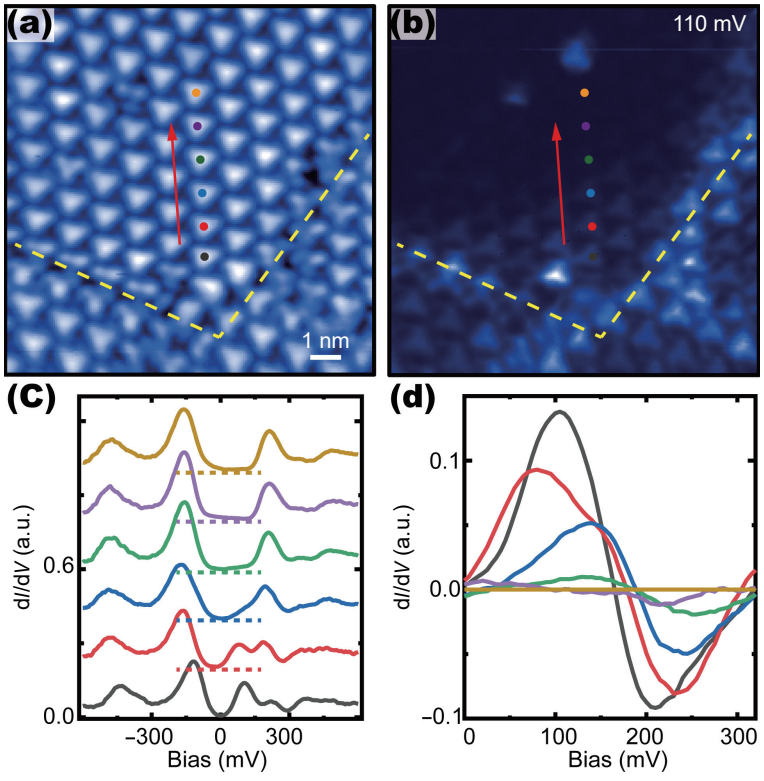

Figure 4 Electron doping evolution near the domain wall. (a) A 12 nm × 12 nm topography with an insulating domain. Yellow dash lines indicate the bottom metallic domain walls. (b) The corresponding dI/dV map at 110 mV. (c) A series of dI/dV spectra taken at the colored dot in (a) (V_b = −600 mV, I_t = 500 pA). (d) The electron-doped in-gap state obtained by subtracting the yellow dI/dV spectra for each dI/dV spectrum in (c).

1T-TaS_2. Intercalated Cu atoms contribute a homogenous electronic doping (rigid chemical shift) rather than local carriers to the 1T-TaS_2 layer from the homogeneous metallic state in each domain. The spatial evolution reveals that the extra doped electron originates from the metallic domain wall. However, this spatial evolution of the doped state has never been observed near the metallic domain walls in the pristine 1T-TaS_2. The super-lattice constant between SDs is several times longer than the atomic lattice in cuprate, which may hinder this phenomenon in pristine 1T-TaS_2. The intercalated Cu atoms strengthen the interaction between different SDs, extending the extra electrons' influence area of the metallic domain wall.

Recently there have been revived interests in the origin of the insulating gap near the Fermi level in pristine samples [10–12]. Some evidence indicates it could be a bandgap considering the stacking order [13–15]. On the other hand, the stacking order effect has been extensively explored as a perturbation in 1T-TaS_2 [25], concluding that the ground insulating state is a Mott insulator which different stacking orders can perturb. However, no noticeable stacking order effect is observed in metallic domains in Cu-intercalated 1T-TaS_2. The intercalated Cu atoms in 1T-TaS_2 inevitably change the stacking orders compared with that in the pristine sample. There are two possible reasons we do not observe the stacking order effect. The global charge transfer between Cu and TaS_2 layer suppresses the Mott insulating state in TaS_2 layers. Secondly, the slight lattice expansion in the *c*-axis may weaken the interlayer coupling and suppress the stacking order effect. The intriguing electronic evolution near the domain wall reveals an electron doping process in the standard Hubbard model [36]. It also demonstrates that the insulating gap is still a strong correlation Mott gap. External parameters like doping, pressure, etc., can be applied to explore exotic electronic states such as superconductor, quantum spin liquid [4, 5, 37].

3 Conclusions

In summary, we performed a comprehensive STM study to understand the role of intercalated Cu atoms in 1T-TaS_2. The intercalated Cu atoms provide a general charge transfer to 1T-TaS_2 and induce metallic domains in the system. We found two distinctive electronic modulations near defective SDs and domain walls, reproducible in different samples. It demonstrated that the intercalated Cu atoms act as a medium to enhance the interaction between SDs and extend the influence area of extra doped electrons. The intriguing electronic evolution also solidified the Mott insulating nature in 1T-TaS_2. Understanding the role of intercalated Cu atoms will motivate searching for exotic phenomena like superconductivity in this system.

4 Methods

4.1 Sample growth

Crystalline 1T-TaS_2 specimens were grown using a CVT method with iodine as a transport agent. First, sealed quartz ampules with pre-reacted powders were sealed and heated in a two-zone furnace. Crystallization was achieved using a temperature gradient of 1,223 and 1,173 K. Finally, the ampules were furnace-cooled to room temperature.

4.2 STM measurement

STM measurements were performed at liquid nitrogen temperature in a commercial ultra-high vacuum system (USM-1500). Samples were cleaved *in situ* and transferred to the STM header immediately. Tungsten tips were calibrated on a clean Au (111) surface in advance. STM topographical images were acquired under bias voltage −600 mV and setpoint 500 pA unless specific point out. The dI/dV spectra were taken by the standard lock-in method with 10 mV and 1,217.3 Hz modulation.

4.3 ADF-STEM characterization

ADF-STEM images were carried out in a JEOL JEM-ARM 300F

microscope equipped with aberration-corrector and operated at an acceleration voltage of 300 kV. ADF-STEM images were recorded in ten-second interval with a frame size of 1,024 × 1,024 pixels (corresponding to 10 nm × 10 nm) and a pixel dwell time of 10 μs. The semi-convergence angle of the incident electron probe was set to 24 mrad, and the detection semi-angle of the ADF detector was 63–200 mrad. ADF-STEM images were analyzed after a drift correction and Gaussian filtering for a better signal-to-noise (S/N) ratio. All the STEM images were carried out at room temperature.

Acknowledgements

Dr. Yonghui Zheng and Prof. Yan Cheng at East China Normal University were acknowledged for their kind assistance on the access to FIB and ADF-STEM used in this study. This work was supported by the National Key Research and Development Program (No. 2019YFA0308602), the Key Research and Development Program of Zhejiang Province, China (No. 2021C01002), Vacuum Interconnected Nanotech Workstation (Nano-X) (B2004) and the Fundamental Research Funds for the Central Universities in China. D. D. and C. J. thank the National Natural Science Foundation of China (Nos. NSFC-51772265 and NSFC-61721005), J. G., W. W., X. L., W. L., and Y. S. thank the support of the National Key Research and Development Program (No. 2016YFA0300404), the National Natural Science Foundation of China (Nos. NSFC-11674326 and NSFC-11874357), the Joint Funds of the National Natural Science Foundation of China, and the Chinese Academy of Sciences' Large-scale Scientific Facility (Nos. U1832141, U1932217, and U2032215).

References

[1] Wilson, J. A.; Di Salvo, F. J.; Mahajan, S. Charge-density waves and superlattices in the metallic layered transition metal dichalcogenides. *Adv. Phys.* **1975**, *24*, 117–201.

[2] Fazekas, P.; Tosatti, E. Electrical, structural and magnetic properties of pure and doped 1T-TaS_2. *Philos. Mag. B* **1979**, *39*, 229–244.

[3] Kim, J. J.; Yamaguchi, W.; Hasegawa, T.; Kitazawa, K. Observation of Mott localization gap using low temperature scanning tunneling spectroscopy in commensurate 1T-TaS_2. *Phys. Rev. Lett.* **1994**, *73*, 2103–2106.

[4] Law, K. T.; Lee, P. A. 1T-TaS_2 as a quantum spin liquid. *Proc. Natl. Acad. Sci. USA.* **2017**, *114*, 6996–7000.

[5] Sipos, B.; Kusmartseva, A. F.; Akrap, A.; Berger, H.; Forró, L.; Tutiš, E. From Mott state to superconductivity in 1T-TaS_2. *Nat. Mater.* **2008**, *7*, 960–965.

[6] Ang, R.; Tanaka, Y.; Ieki, E.; Nakayama, K.; Sato, T.; Li, L. J.; Lu, W. J.; Sun, Y. P.; Takahashi, T. Real-space coexistence of the melted Mott state and superconductivity in Fe-substituted 1T-TaS_2. *Phys. Rev. Lett.* **2012**, *109*, 176403.

[7] Liu, Y.; Ang, R.; Lu, W. J.; Song, W. H.; Li, L. J.; Sun, Y. P. Superconductivity induced by Se-doping in layered charge-density-wave system 1T-$TaS_{2-x}Se_x$. *Appl. Phys. Lett.* **2013**, *102*, 192602.

[8] Qiao, S.; Li, X. T.; Wang, N. Z.; Ruan, W.; Ye, C.; Cai, P.; Hao, Z. Q.; Yao, H.; Chen, X. H.; Wu, J. et al. Mottness collapse in 1T-$TaS_{2-x}Se_x$ transition-metal dichalcogenide: An interplay between localized and itinerant orbitals. *Phys. Rev. X* **2017**, *7*, 041054.

[9] Yu, Y. J.; Yang, F. Y.; Lu, X. F.; Yan, Y. J.; Cho, Y. H.; Ma, L. G.; Niu, X. H.; Kim, S.; Son, Y. W.; Feng, D. L. et al. Gate-tunable phase transitions in thin flakes of 1T-TaS_2. *Nat. Nanotechnol.* **2015**, *10*, 270–276.

[10] Ritschel, T.; Trinckauf, J.; Koepernik, K.; Büchner, B.; Zimmermann, M. V.; Berger, H.; Joe, Y. I.; Abbamonte, P.; Geck, J. Orbital textures and charge density waves in transition metal dichalcogenides. *Nat. Phys.* **2015**, *11*, 328–331.

[11] Lee, S. H.; Goh, J. S.; Cho, D. Origin of the insulating phase and first-order metal-insulator transition in 1T-TaS_2. *Phys. Rev. Lett.* **2019**, *122*, 106404.

[12] Shin, D.; Tancogne-Dejean, N.; Zhang, J.; Okyay, M. S.; Rubio, A.; Park, N. Identification of the Mott insulating charge density wave state in 1T-TaS_2. *Phys. Rev. Lett.* **2021**, *126*, 196406.

[13] Butler, C. J.; Yoshida, M.; Hanaguri, T.; Iwasa, Y. Mottness versus unit-cell doubling as the driver of the insulating state in 1T-TaS_2. *Nat. Commun.* **2020**, *11*, 2477.

[14] Wang, Y. D.; Yao, W. L.; Xin, Z. M.; Han, T. T.; Wang, Z. G.; Chen, L.; Cai, C.; Li, Y.; Zhang, Y. Band insulator to Mott insulator transition in 1T-TaS_2. *Nat. Commun.* **2020**, *11*, 4215.

[15] Stahl, Q.; Kusch, M.; Heinsch, F.; Garbarino, G.; Kretzschmar, N.; Hanff, K.; Rossnagel, K.; Geck, J.; Ritschel, T. Collapse of layer dimerization in the photo-induced hidden state of 1T-TaS_2. *Nat. Commun.* **2020**, *11*, 1247.

[16] Wan, J. Y.; Lacey, S. D.; Dai, J. Q.; Bao, W. Z.; Fuhrer, M. S.; Hu, L. B. Tuning two-dimensional nanomaterials by intercalation: Materials, properties, and applications. *Chem. Soc. Rev.* **2016**, *45*, 6742–6765.

[17] Wang, Z. Y.; Li, R. L.; Su, C. L.; Loh, K. P. Intercalated phases of transition metal dichalcogenides. *SmartMat* **2020**, *1*, e1013.

[18] Liu, X. C.; Zhao, S. Y.; Sun, X. P.; Deng, L. Z.; Zou, X. L.; Hu, Y. C.; Wang, Y. X.; Chu, C. W.; Li, J.; Wu, J. J. et al. Spontaneous self-intercalation of copper atoms into transition metal dichalcogenides. *Sci. Adv.* **2020**, *6*, eaay4092.

[19] Zhang, J. S.; Sun, J.; Li, Y. B.; Shi, F. F.; Cui, Y. Electrochemical control of copper intercalation into nanoscale Bi_2Se_3. *Nano Lett.* **2017**, *17*, 1741–1747.

[20] Wang, P. D.; Khan, R.; Liu, Z. F.; Zhang, B.; Li, Y. L.; Wang, S.; Wu, Y. B.; Zhu, H. E.; Liu, Y.; Zhang, G. B. et al. A Non-rigid shift of band dispersions induced by Cu intercalation in 2H-$TaSe_2$. *Nano Res.* **2020**, *13*, 353–357.

[21] Novello, A. M.; Spera, M.; Scarfato, A.; Ubaldini, A.; Giannini, E.; Bowler, D. R.; Renner, C. Stripe and short range order in the charge density wave of 1T-Cu_xTaSe_2. *Phys. Rev. Lett.* **2017**, *118*, 017002.

[22] Yan, S. C.; Iaia, D.; Morosan, E.; Fradkin, E.; Abbamonte, P.; Madhavan, V. Influence of domain walls in the incommensurate charge density wave state of Cu intercalated 1T-$TaSe_2$. *Phys. Rev. Lett.* **2017**, *118*, 106405.

[23] Qian, D.; Hsieh, D.; Wray, L.; Morosan, E.; Wang, N. L.; Xia, Y.; Cava, R. J.; Hasan, M. Z. Emergence of Fermi pockets in a new excitonic charge-density-wave melted superconductor. *Phys. Rev. Lett.* **2007**, *98*, 117007.

[24] Zhang, K. W.; Yang, C. L.; Lei, B.; Lu, P. C.; Li, X. B.; Jia, Z. Y.; Song, Y. H.; Sun, J.; Chen, X. H.; Li, J. X. et al. Unveiling the charge density wave inhomogeneity and pseudogap state in 1T-$TaSe_2$. *Sci. Bull.* **2018**, *63*, 426–432.

[25] Wu, Z. X.; Bu, K. L.; Zhang, W. H.; Fei, Y.; Zheng, Y.; Gao, J. J.; Luo, X.; Liu, Z.; Sun, Y. P.; Yin, Y. Effect of stacking order on the electronic state of 1T-TaS_2. *Phys. Rev. B.* **2022**, *105*, 035109.

[26] Bu, K. L.; Zhang, W. H.; Fei, Y.; Wu, Z. X.; Zheng, Y.; Gao, J. J.; Luo, X.; Sun, Y. P.; Yin, Y. Possible strain induced Mott gap collapse in 1T-TaS_2. *Commun. Phys.* **2019**, *2*, 146.

[27] Lahoud, E.; Meetei, O. N.; Chaska, K. B.; Kanigel, A.; Trivedi, N. Emergence of a novel pseudogap metallic state in a disordered 2D Mott insulator. *Phys. Rev. Lett.* **2014**, *112*, 206402.

[28] Lee, P. A.; Ramakrishnan, T. V. Disordered electronic systems. *Rev. Mod. Phys.* **1985**, *57*, 287–337.

[29] Szabo, J. C.; Lee, K.; Madhavan, V.; Trivedi, N. Local spectroscopies reveal percolative metal in disordered Mott insulators. *Phys. Rev. Lett.* **2020**, *124*, 137402.

[30] Regan, E. C.; Wang, D. Q.; Jin, C. H.; Utama, M. I. B.; Gao, B. N.; Wei, X.; Zhao, S. H.; Zhao, W. Y.; Zhang, Z. C.; Yumigeta, K. et al. Mott and generalized Wigner crystal states in WSe_2/WS_2 Moiré superlattices. *Nature* **2020**, *579*, 359–363.

[31] Zhang, Y.; Gao, F.; Gao, S. W.; He, L. Tunable magnetism of a single-carbon vacancy in graphene. *Sci. Bull.* **2020**, *65*, 194–200.

[32] Cho, D.; Gye, G.; Lee, J.; Lee, S. H.; Wang, L. H.; Cheong, S. W.; Yeom, H. W. Correlated electronic states at domain walls of a Mott-

charge-density-wave insulator 1T-TaS_2. *Nat. Commun.* **2017**, *8*, 392.
[33] Skolimowski, J.; Gerasimenko, Y.; Žitko, R. Mottness collapse without metallization in the domain wall of the triangular-lattice Mott insulator 1T-TaS_2. *Phys. Rev. Lett.* **2019**, *122*, 036802.
[34] Park, J. W.; Lee, J.; Yeom, H. W. Zoology of domain walls in quasi-2D correlated charge density wave of 1T-TaS_2. *npj Quantum Mater.* **2021**, *6*, 32.
[35] Ye, C.; Cai, P.; Yu, R. Z.; Zhou, X. D.; Ruan, W.; Liu, Q. Q.; Jin, C. Q.; Wang, Y. Y. Visualizing the atomic-scale electronic structure of the $Ca_2CuO_2Cl_2$ Mott insulator. *Nat. Commun.* **2013**, *4*, 1365.
[36] Eskes, H.; Meinders, M. B. J.; Sawatzky, G. A. Anomalous transfer of spectral weight in doped strongly correlated systems. *Phys. Rev. Lett.* **1991**, *67*, 1035–1038.
[37] Klanjšek, M.; Zorko, A.; Žitko, R.; Mravlje, J.; Jagličić, Z.; Biswas, P. K.; Prelovšek, P.; Mihailovic, D.; Arčon, D. A high-temperature quantum spin liquid with polaron spins. *Nat. Phys.* **2017**, *13*, 1130–1134.